

Anomalous magnetic exchange in a dimerized quantum magnet composed of unlike spin species

S. P. M. Curley¹, B. M. Huddart², D. Kamenskyi^{3,4}, M. J. Coak¹, R. C. Williams¹, S. Ghannadzadeh⁵, A. Schneider⁶, S. Okubo⁴, T. Sakurai⁴, H. Ohta⁴, J. P. Tidey⁷, D. Graf⁸, S. J. Clark², S. J. Blundell⁵, F. L. Pratt⁹, M. T. F. Telling⁹, T. Lancaster^{2,*}, J. L. Manson^{10,†} and P. A. Goddard^{1,‡}

¹*Department of Physics, University of Warwick, Gibbet Hill Road, Coventry CV4 7AL, United Kingdom*

²*Centre for Materials Physics, Department of Physics, Durham University, Durham DH1 3LE, United Kingdom*

³*Experimental Physics V, Center for Electronic Correlations and Magnetism, Institute of Physics, University of Augsburg, 86135 Augsburg, Germany*

⁴*Molecular Photoscience Research Center, Kobe University, 657-8501 Kobe, Japan*

⁵*Department of Physics, Clarendon Laboratory, Oxford University, Parks Road, Oxford OX1 3PU, United Kingdom*

⁶*Experimental Physics VI, Center for Electronic Correlations and Magnetism, Institute of Physics, University of Augsburg, 86135 Augsburg, Germany*

⁷*Department of Chemistry, University of Warwick, Gibbet Hill, Coventry CV4 7AL, United Kingdom*

⁸*National High Magnetic Field Laboratory, Florida State University, Tallahassee, Florida 32310, USA*

⁹*ISIS Facility, Rutherford Appleton Laboratory, Chilton, Oxfordshire OX11 0QX, United Kingdom*

¹⁰*Department of Chemistry and Biochemistry, Eastern Washington University, Cheney, Washington 99004, USA*



(Received 3 September 2021; accepted 22 November 2021; published 30 December 2021)

We present here a study of the magnetic properties of the antiferromagnetic dimer material $\text{CuVOF}_4(\text{H}_2\text{O})_6 \cdot \text{H}_2\text{O}$, in which the dimer unit is composed of two different $S = 1/2$ species, Cu(II) and V(IV). An applied magnetic field of $\mu_0 H_{c1} = 13.1(1)$ T is found to close the singlet-triplet energy gap, the magnitude of which is governed by the antiferromagnetic intradimer $J_0 \approx 21$ K, and interdimer $J' \approx 1$ K, exchange energies, determined from magnetometry and electron-spin resonance measurements. The results of density functional theory (DFT) calculations are consistent with the experimental results. The DFT calculations predict antiferromagnetic coupling along all nearest-neighbor bonds, with the magnetic ground state comprising spins of different species aligning antiparallel to one another, while spins of the same species are aligned parallel. The magnetism in this system cannot be accurately described by the overlap between localized V orbitals and magnetic Cu orbitals lying in the Jahn-Teller (JT) plane, with a tight-binding model based on such a set of orbitals incorrectly predicting that interdimer exchange should be dominant. DFT calculations indicate significant spin density on the bridging oxide, suggesting instead an unusual mechanism in which intradimer exchange is mediated through the O atom on the Cu(II) JT axis.

DOI: [10.1103/PhysRevB.104.214435](https://doi.org/10.1103/PhysRevB.104.214435)

I. INTRODUCTION

Cooperative phenomena in materials known to exhibit quantum critical points (QCPs) have been the subject of consistent interest in condensed matter physics [1–3]. In particular, systems of antiferromagnetically (AFM) coupled $S = 1/2$ dimers have been known to exhibit two magnetic-field-induced phase transitions; the first of which, at least, involves the system passing through a QCP which, under certain conditions, belongs to the Bose-Einstein condensate (BEC) universality class [3,4].

In zero field (ZF) and at low temperatures, weakly interacting $S = 1/2$ AFM dimers exist in a state of quantum disorder, the ground state being composed of a sea of spin singlets ($S = 0$) situated against a backdrop of quantum fluctuations. Above

this singlet ground state resides a degenerate excited triplet state ($S = 1$), with the size of the singlet-triplet energy gap dictated by the strength of the intradimer AFM Heisenberg exchange interaction $J_0 > 0$. The presence of any interdimer exchange J' serves to disperse the excited triplet, giving a band of excitations and reducing the size of the singlet-triplet energy gap relative to the case for an isolated dimer.

Upon application of an external field, the system moves through the first QCP, at H_{c1} , as the Zeeman interaction splits the degenerate $S = 1$ triplet and lowers the energy of the $S_z = +1$ state below that of the $S = 0$ singlet ground state, such that at H_{c1} the system enters a long-range XY-AFM ordered state. Under certain conditions, the triplet excitations in the ordered state can be described as bosonic quasiparticles [3]. Further application of field eventually fully polarizes the spins along the field direction, as the system enters a ferromagnetic (FM) saturated state above H_{c2} .

In order for the excited triplet state to effectively map onto a BEC of magnons picture, the transverse component of the spins must spontaneously break the rotational $O(2)$ symmetry

*tom.lancaster@durham.ac.uk

†jmanson@ewu.edu

‡p.goddard@warwick.ac.uk

[analogous to the $U(1)$ symmetry present in an atomic BEC] of the system at H_{c1} [5]. Thus, any term which breaks the rotational symmetry of the spin Hamiltonian prohibits the system from being described within the BEC universality class [6]. Dimers which exhibit an excited triplet state where the crystal structure breaks the $O(2)$ symmetry have been reported previously [7,8].

However, we present here the magnetic properties of the dimer system $\text{CuVOF}_4(\text{H}_2\text{O})_6 \cdot \text{H}_2\text{O}$ [9], where the rotational symmetry is broken not only by the structure, but also by the spin species which make up the dimer unit. Within an applied magnetic field, the system can be modeled as a lattice of weakly coupled $S = 1/2$ AFM dimers interacting via Heisenberg exchange, with the magnetic properties summarized by

$$\mathcal{H} = J_0 \sum_i \hat{\mathbf{S}}_{1,i} \cdot \hat{\mathbf{S}}_{2,i} + \sum_{\langle mni j \rangle} J'_{mni j} \hat{\mathbf{S}}_{m,i} \cdot \hat{\mathbf{S}}_{n,j} - g\mu_B \mu_0 H \sum_i \hat{S}_{m,i}^z, \quad (1)$$

where i and j denote dimers and $m, n = 1, 2$ label magnetic sites [4,5]. We note that as the dimer-unit lacks a center of inversion symmetry, there is the possibility of an additional Dzyaloshinskii-Moriya interaction (DMI) term in the Hamiltonian of the form $\mathbf{D} \cdot (\mathbf{S}_1 \times \mathbf{S}_2)$. The magnitude of the DM term can be estimated from the departure of the g factor from the free electron value $|D| \sim (\Delta g/g)J_0$ [10] and is typically expected to be small as observed in the dimer $\text{Ba}_3\text{Cr}_2\text{O}_8$ where $(\Delta g/g)J_0 \sim 1$ K and $J_0 = 27.6(2)$ K [11,12].

In this paper we present ZF muon-spin relaxation data that indicate an absence of magnetic order down to temperatures of 100 mK, typical behavior for a system of weakly interacting dimers [4]. In addition, radio-frequency (RF) susceptibility measurements confirm the existence of two field-induced phase transitions akin to behavior observed in other BEC class dimers [12,13], and allow the magnetic phase diagram to be elucidated.

Due to the exceptional energy resolution and relevant frequency range, electron-spin resonance (ESR) is one of the most appropriate experimental techniques to probe the singlet-triplet excitations. Such transitions have been observed by high-frequency ESR in many AFM spin dimers, such as: $\text{SrCu}_2(\text{BO}_3)_2$ [14,15] and CuTe_2O_5 [16] based on Cu(II) ($3d^9$, $S = 1/2$) ions; $\text{Ba}_3\text{Cr}_2\text{O}_8$ [17,18] and $\text{Sr}_3\text{Cr}_2\text{O}_8$ [18,19] based on Cr^{3+} ($3d^1$, $S = 1/2$). Here ESR measurements directly observe the closure of the singlet-triplet energy gap in $\text{CuVOF}_4(\text{H}_2\text{O})_6 \cdot \text{H}_2\text{O}$ and highlight several excitations in the system, including a so-far-unidentified resonance which appears to be unique to this system.

As detailed in Ref. [9], $\text{CuVOF}_4(\text{H}_2\text{O})_6 \cdot \text{H}_2\text{O}$ is composed of the two unlike $S = 1/2$ ions, Cu(II) ($3d^9$) and V(IV) ($3d^1$), linked via a lambda-shaped Cu-O-V bond. Work in Ref. [9] showed that the formation of this Cu-O-V bond relies on the Jahn-Teller (JT) distortion of the Cu(II) octahedra, and replacing Cu(II) with other $M(\text{II})$ transition-metal ions ($M = \text{Ni, Zn, Co}$) results in the $M(\text{II})$ and V(IV) ions forming isolated octahedra. In this work we demonstrate that the JT-active Cu is not only responsible for the polar structure, but also the low-dimensional magnetism in the system. Density functional theory calculations show that the unlike spin species likely

play an important role in the intradimer exchange mechanism in this compound, which appears to be distinct from the exchange coupling picture, typical for Cu(II) magnets, of overlapping d orbitals within the JT plane.

II. RESULTS

A. Structure

Single-crystal x-ray diffraction data indicate $\text{CuVOF}_4(\text{H}_2\text{O})_6 \cdot \text{H}_2\text{O}$ crystallizes into an orthorhombic structure with polar space-group $Pna2_1$, in agreement with Ref. [9]. (A full structural report can be found in the Supplemental Material (SM) [20] which also includes Refs. [21–23]) The magnetic structure of $\text{CuVOF}_4(\text{H}_2\text{O})_6 \cdot \text{H}_2\text{O}$ is based on a lattice of weakly interacting antiferromagnetically coupled $S = 1/2$ dimers. The dimeric-unit itself is composed of two differing $S = 1/2$ ions, V(IV) and Cu(II) , both of which reside in octahedral environments of the form VF_4O_2 , Fig. 1(a), and CuO_6 , Fig. 1(b). Figure 1(c) shows that the Cu(II) and V(IV) ions are linked via a bent Cu-O-V bond [with a Cu-O-V bond-angle of $142.87(5)^\circ$ and though-bond distance between the Cu and V ions of $3.942(2)$ Å] and by a single $\text{Cu-O-H} \cdots \text{F-V}$ bond.

Where the Jahn-Teller axis of the Cu directs along the bridging Cu-O bond, the unpaired electron ($3d^9$) of the metal center is expected to reside in the $d_{x^2-y^2}$ orbital, oriented in the plane perpendicular to this bond and directed along the shorter Cu-O bonds which lie within the JT plane. For V, density functional theory (DFT) calculations (outlined below) indicate significant spin density between the V-F bonds, also perpendicular to the Cu-O-V bond. It should be noted that JT-active Cu(II) systems often exhibit extreme low dimensionality, as the reduced orbital overlap along the JT direction typically leads to strong superexchange interactions only along pathways perpendicular to the JT axis, such as in the quasi-two-dimensional $[\text{Cu}(\text{HF}_2)(\text{pyz})_2]\text{SbF}_6$ [24] and quasi-one-dimensional $\text{Cu}(\text{NO}_3)_2(\text{pyz})_3$ [25] ($\text{pyz} = \text{pyrazine} = \text{C}_4\text{H}_4\text{N}_2$) molecule-based magnets. As the magnetic orbitals of both the Cu and V lie within the plane of the equatorial ligands of each octahedral environment, one might expect that the minimal orbital overlap along the Cu-O-V bond direction would lead to the intradimer exchange coupling (J_0) being mediated along the intradimer $\text{Cu-O-H} \cdots \text{F-V}$ H-bond pathway, seen in Fig. 1(c). H bonds have previously been shown to be highly effective mediators of superexchange interactions in low-dimensional magnets, such as $[\text{CuF}_2(\text{H}_2\text{O})_2(\text{pyz})]$ [26] and $\text{CuSO}_4(\text{C}_2\text{H}_8\text{N}_2) \cdot 2\text{H}_2\text{O}$ [27]. However, it is shown later that this is not the case for this material.

Weak H bonds between the dimers form a complex 3D interdimer network, outlined in detail in [9]. Only the interdimer H bonds between equatorial ligands are expected to mediate significant magnetic exchange, as the magnetic orbitals of both transition-metal ion species lie within the plane of the equatorial ligands, with no spin density located on the axial water ligands of either species (see DFT below). As such, the primary interdimer exchange is expected to act within the bc plane via the H-bond network shown in Fig. 1(d), resulting in each dimer having four nearest dimer neighbors $n = 4$. There may also be some very weak exchange along a (J''). Most

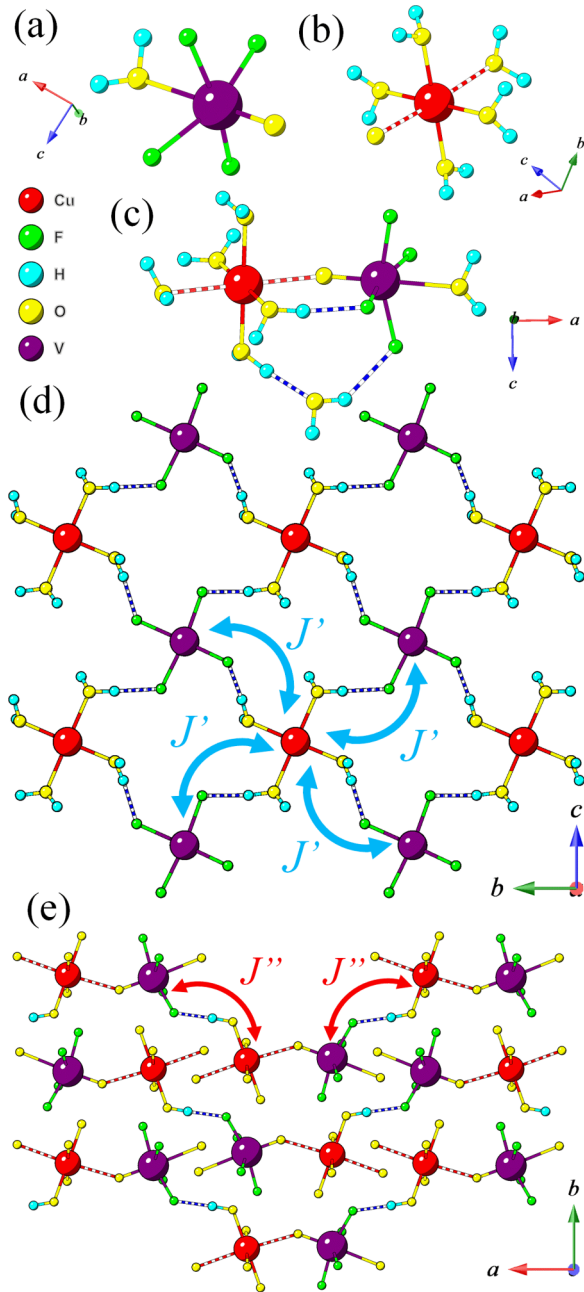


FIG. 1. Local octahedral environment of (a) V(IV) and (b) Cu(II). Red-striped bonds indicate the Jahn-Teller axis of the Cu(II) octahedra. (c) Dimer unit with intradimer H bonds (blue-striped bonds) through equatorial ligands and uncoordinated water molecule. (d) Interdimer H-bond network within the bc plane expected to mediate primary interdimer exchange (J'). Uncoordinated waters are omitted for clarity. (e) Packing of the dimers along a showing equatorial H bonds expected to mediate secondary interdimer exchange (J'') assumed to be very small; see text. H bonds between axial and uncoordinated waters omitted for clarity. Structure is determined from single-crystal x-ray diffraction data collected at 150 K; see the SM [20].

H-bond pathways along a involve a JT (pseudo-JT) axis of the Cu (V), such that the equatorial H bonds highlighted in Fig. 1(e) (which bridge adjacent Cu and V ions along a) are the most probable J'' exchange pathways. It should be noted

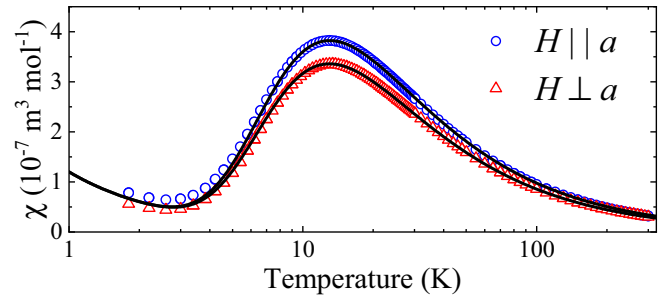


FIG. 2. Quasistatic DC-field magnetic susceptibility $\chi(T)$ for an orientated single crystal of $\text{CuVOF}_4(\text{H}_2\text{O})_6 \cdot \text{H}_2\text{O}$ measured in an applied field of $\mu_0 H = 0.1$ T. Solid lines are a global fit of Eq. (2) to both data sets as described in the text.

that adjacent Cu octahedra throughout the lattice are arranged in a staggered fashion (likewise for adjacent V octahedra), as seen in Fig. 1(e), indicating a staggered g tensor within the system.

B. Magnetometry

1. SQUID magnetometry

Figure 2 shows the static magnetic susceptibility [$\chi(T)$] for a single crystal of $\text{CuVOF}_4(\text{H}_2\text{O})_6 \cdot \text{H}_2\text{O}$ with field orientated parallel and perpendicular to the crystallographic a axis (which lies close to parallel with the Cu–O–V bond). Upon decreasing temperature, $\chi(T)$ data in both orientations rise to a broad hump centered around 15 K, decrease down to $T \approx 3$ K, and then exhibit a slight upturn at $T < 3$ K; behavior typical of AFM coupled spin-half dimers. Over the measured temperature range, $1.8 \leq T \leq 300$ K, $\chi(T)$ can well be described using a Bleaney-Bowers model with mean-field interactions $\chi_b(T)$ [12,28] of the form

$$\chi = (1 - \rho)\chi_b(T) + \rho\chi_{\text{pm}}(T), \quad (2)$$

where $\chi_{\text{pm}}(T)$ models the low-temperature paramagnetic tail and ρ captures the fraction of the sample attributable to uncoupled $S = 1/2$ spins due to impurities and broken dimers, or, possibly arising from the staggering of the local g tensor as seen in staggered $S = 1/2$ chains [29,30] (the full form of Eq. (2) can be found in the SM [20]). The $\chi(T)$ data sets were fit simultaneously sharing J_0 , J' , and ρ as global parameters, but with g factors free to vary for each data set. The resultant fit is shown in Fig. 2 (solid lines) and returns parameters of $J_0 = 21.3(1)$ K, $J' = 1.3(1)$ K (taking $n = 4$ from the structure), and $\rho = 2.5(1)\%$. The extracted g factors of $g_a = 2.1(1)$ and $g_{bc} = 2.0(1)$ are in excellent agreement with the values determined from ESR measurements discussed below.

2. Radio frequency susceptibility

Figure 3(a) shows the field dependence of the differential magnetization (dM/dH) measured at various temperatures for a single crystal of $\text{CuVOF}_4(\text{H}_2\text{O})_6 \cdot \text{H}_2\text{O}$, with field parallel to a , measured using a radio-frequency oscillator technique [31–33]. Measurements were performed using quasistatic fields to mitigate magnetocaloric effects known to be present in dimer systems in rapidly changing magnetic fields [34,35].

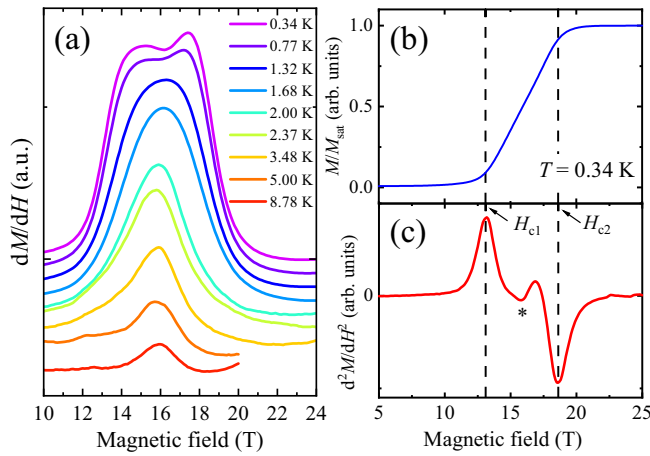


FIG. 3. (a) Dynamic susceptibility dM/dH measured at several temperatures using radio-frequency (RF) susceptometry with field parallel to the a axis. Data are offset at each temperature for clarity. Normalized magnetization (M/M_{sat}) (b) and its second derivative (d^2M/dH^2) (c) measured at $T = 0.34$ K extracted from the RF susceptometry. The positions of the first and second critical fields, H_{c1} and H_{c2} , derived from d^2M/dH^2 , are marked with dashed lines in (b) and (c). The minimum feature in d^2M/dH^2 , discussed in text, is marked with an asterisk.

At low temperatures, dM/dH exhibits two peaklike features centered around 14.5 and 18.5 T, which coalesce and become unresolvable as separate peaks for $1.68 < T \leq 2$ K. Typically in $S = 1/2$ dimer systems, sharp cusps are observed in dM/dH at the critical fields H_{c1} and H_{c2} [4,34]. The reason for the broad nature of the features in dM/dH here is unknown, but could arise due to H-bond disorder within the complex interdimer exchange network, giving rise to a distribution in the superexchange between neighboring transition metal sites and a smearing of the transition features in dM/dH [36].

The magnetization $M(H)$, shown in Fig. 3(b), is extracted by integrating the measured dM/dH response. The low-temperature $M(H)$ response is typical for a system of weakly interacting $S = 1/2$ AFM dimers [4,13], with a sharp upturn at $H = H_{c1}$ corresponding to the closing of the singlet-triplet energy gap and a leveling off at $H = H_{c2}$ indicating the spins are fully polarized along the field direction at H_{c2} .

Figure 3(c) shows the peaks in the second derivative of the $M(H)$ (d^2M/dH^2) that we use to track the positions of H_{c1} and H_{c2} , as done previously for other dimer systems [37]. The minimum in d^2M/dH^2 between the two critical fields, marked with an asterisk, disappears for $1.68 < T \leq 2$ K. This is the same temperature range where the two peak features in dM/dH coalesce [Fig. 3(a)] and provides a consistent estimate for the temperature limit beyond which the two critical fields can no longer be resolved.

C. Electron-spin resonance

1. X-band ESR

Figure 4 displays the low-temperature electron-spin resonance (ESR) spectra (the derivative of the absorption) measured at a frequency of $\nu = 9.35$ GHz. The top panel

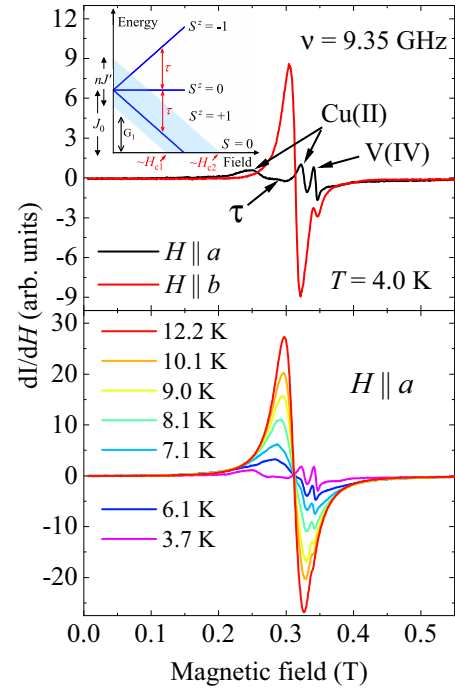


FIG. 4. Top panel shows X-band ESR spectra of $\text{CuVOF}_4(\text{H}_2\text{O})_6 \cdot \text{H}_2\text{O}$ for $H \parallel a$ (black curve) and $H \parallel b$ (red curve) measured at 4.0 K. Inset shows schematic energy-level diagram for interacting $S = 1/2$ dimers. Bottom panel shows the temperature evolution of ESR spectra for $H \parallel a$.

compares spectra for field along the a and b axis. For field along a (black curve) the spectrum consists of four peaks indicated with arrows. Upon increasing temperature the magnitude of the three most intense peaks diminishes, indicating these resonances can be attributed to free paramagnetic ions with g factors: 1.95, originating from V(IV); 2.37, originating from Cu(II); and 2.05, which is likely due to Cu(II) impurities. However, we note the additional possibility of an uncompensated moment on the dimer due to the nonidentical spins. This would likely manifest as a g factor between that of the Cu and V values. The weak peak marked τ corresponds to transitions ($\Delta S_z = \pm 1$) that occur within the excited triplet state. For field along b only two peaks can be resolved: that arising from V(IV) with $g = 1.965$ and a very intense absorption with $g = 2.15$ which derives from transitions within the triplet and Cu(II) impurities. These results are in agreement with the magnetometry, which also suggests the presence of a small component resembling free $S = 1/2$ ions within the sample.

The temperature evolution of the ESR spectra with $H \parallel a$ is shown in the bottom panel of Fig. 4. As expected, upon increasing temperature the intensity of the transitions within the excited triplet (τ peak) increases rapidly as their population increases, while the intensities of the other transition peaks decreases. Above 10 K, the triplet transitions dominate the excitation spectrum exhibiting a maximum intensity at 17 K, in agreement with the hump around 15 K seen in $\chi(T)$ (Fig. 2 above). At 10 K, the g factor of the τ mode with $H \parallel a$ is 2.14 and grows to 2.155 upon warming to room temperature $T = 295$ K. The g factors along the principal axes are therefore $g_a = 2.145$, $g_b = 2.046$, and $g_c = 2.055$ at

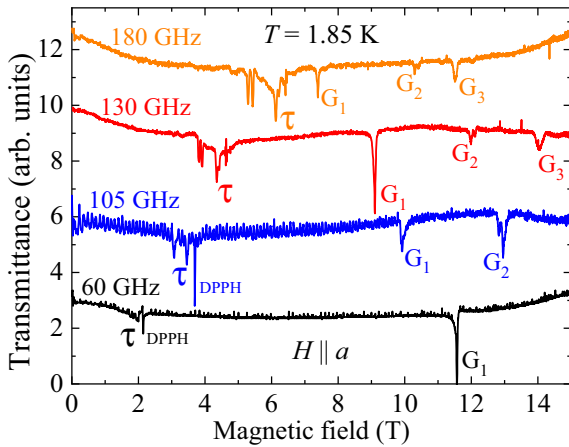


FIG. 5. ESR spectra of $\text{CuVOF}_4(\text{H}_2\text{O})_6 \cdot \text{H}_2\text{O}$ at different radiation frequencies measured at 1.85 K with $H \parallel a$. A sharp peak marked “DPPH” corresponds to the absorption by the field marker compound. The peaks labeled τ and $G_{1,2,3}$ are as described in the text.

20 K and $g_a = 2.155$, $g_b = 2.039$, and $g_c = 2.047$ at room temperature; see the SM [20].

2. High-frequency ESR

Figure 5 shows the ESR spectra measured at frequencies of $\nu = 60, 105, 130,$ and 180 GHz for field applied approximately along the dimer axis ($H \parallel a$) with multiple modes observed in the spectra (τ , G_1 , G_2 , and G_3) that can be categorized based on their field dependence.

The field position of the τ mode, and the several satellite peaks arising from free paramagnetic spins, increases linearly with the radiation frequency $h\nu = g\mu_B\mu_0H$; behavior typical for paramagnetic ions and transitions within the excited triplet of a dimer system. These modes are high-field extensions of the excitations observed in the X-band spectra discussed above.

The G_n modes have a finite energy in zero-field Δ_{G_n} , such that Δ_{G_n} decreases upon increasing field. This is typical behavior of singlet-triplet transitions whose frequency follows $h\nu = h\Delta_{G_n} - g\mu_B\mu_0H$, where Δ_{G_n} corresponds to the energy gap between the $S = 0$ singlet ground state and $S_z = +1$ triplet state. Often, singlet-triplet transitions are forbidden in simple dimers, however, the presence of a nonzero DMI or an alternating g tensor can serve to mix the wave functions of the spin-singlet ground state and spin-triplet excited states, permitting singlet-triplet transitions [17].

Normally, ESR experiments probe transitions at the center of Brillouin zone (Γ point), at $k = 0$. However, under certain circumstances transitions at nonzero k can be observed due to Brillouin zone folding [17,18,38]. Therefore, we assign the most intense mode G_1 to singlet-triplet excitations at the Γ point while the other modes G_2 and G_3 are attributed to similar transitions which occur at nonzero k .

The frequency dependence of the peak positions at 1.85 K is shown in Fig. 6. Solid lines show the best fit of the data obtained using $g = 2.145$ taken from the X-band measurements, the fit returns values of $\Delta_{G_1} = 398(3)$ GHz [19.1(1) K] and $\Delta_{G_2} = 485(3)$ GHz [23.3(1) K].

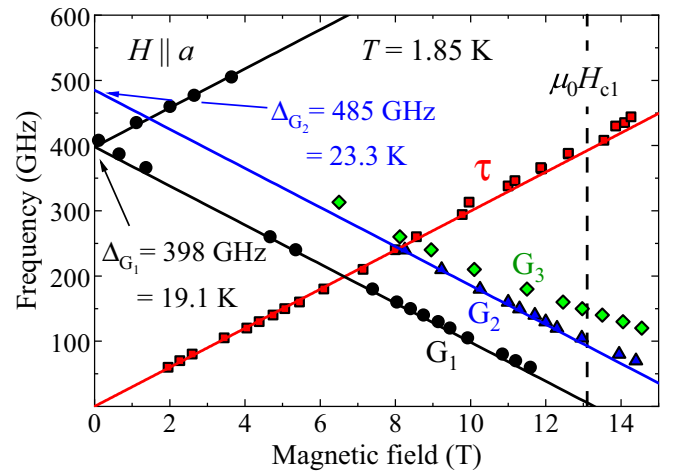


FIG. 6. Frequency-field dependence of the ESR transitions in $\text{CuVOF}_4(\text{H}_2\text{O})_6 \cdot \text{H}_2\text{O}$ measured at 1.85 K with $H \parallel a$. Solid lines are the best fit of the data with $g = 2.145$ as obtained from the X-band measurements (Fig. 4). Dashed line marks the first critical field $\mu_0H_{c1} = 13.1$ K, obtained from RF-susceptometry measurements at $T = 0.34$ K with $H \parallel a$.

Typically, the ESR spectra of similar dimer compounds [17,18] exhibits two modes, Δ_{G_1} and Δ_{G_2} , which provide information about the strength of the intradimer and interdimer coupling. The singlet-triplet zero-field splitting is dictated by the intradimer coupling J_0 while the interdimer interaction J' determines the dispersion of the triplet state. Values of J_0 and J' can be estimated within the random phase approximation [39,40] (where $h\Delta_{G_{1,2}} = J_0 \mp 2J'$ for $n = 4$ nearest neighbors) which returns parameters of $J_0 = 21.0(2)$ K and $J' = 1.0(1)$ K, in excellent agreement with magnetometry data. Extrapolating the G_1 mode to zero-frequency estimates values of $\mu_0H_{c1}^a = 13.3(2)$ T and $\mu_0H_{c1}^b = 14.0(2)$ T for field along the a and b axis, respectively, which is close to the critical field of $13.1(1)$ T, for field along the a axis, extracted from RF susceptometry (dashed line Fig. 6).

The phase transition occurs at the point when the Zeeman interaction closes the singlet-triplet energy gap. Upon increasing field, the singlet-triplet energy gap need not strictly close at the Γ point but may close at another point within the Brillouin zone. While ESR measurements are sensitive to the Γ point, the bulk magnetometry probes the whole Brillouin zone. Thus, the critical fields extracted from ESR data must fall between the magnetic-field range outlined by the values of $H_{c1,2}$ determined from magnetometry measurements, as reported in the dimer compound $\text{Ba}_3\text{Cr}_2\text{O}_8$ [17], and in line with the results in this work.

The observation of a third mode G_3 in the ESR spectrum is unexpected, as only two modes are observed in the ESR spectrum of similar dimer materials [17–19]. While the origin of this mode is presently unclear, further ESR experiments are planned to investigate the possible existence of a DMI, and to elucidate the effect this may have on the field dependence of the dimer energy levels, as outlined in [41].

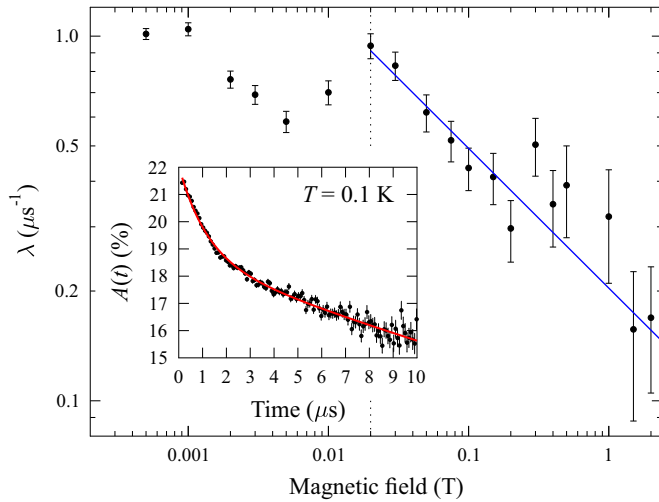


FIG. 7. Field dependence of the longitudinal-field relaxation rate alongside a power-law fit, described in the text, appropriate for diffusive spin transport. Inset: ZF μ^+ SR spectrum measured at $T = 0.1$ K.

D. Muon-spin relaxation

Zero-field positive-muon-spin-relaxation (μ^+ SR) spectra (inset Fig. 7) show very little temperature dependence, and do not show any oscillations in the asymmetry (that would be characteristic of magnetic order) down to 0.1 K; see the SM [20] which also includes Refs. [42–45]. The spectra are instead characterized by exponential relaxation due to fluctuating electronic moments and a slowly relaxing contribution due to muons implanting at sites not sensitive to these electronic moments. The observation of exponential relaxation due to fluctuating electron moments is distinct from the behavior of the $S = 1/2$ dimer system $[\text{Cu}(\text{pyz})_{0.5}(\text{gly})]\text{ClO}_4$ ($\text{gly} = \text{C}_2\text{H}_5\text{NO}_2$), for which only Gaussian relaxation, due to disordered nuclear magnetic moments, is observed [4]. This implies that either the amplitude of the fluctuating field at the muon site is larger in the Cu-V system or (assuming a fast-fluctuation limit typical of this temperature regime) that the characteristic fluctuation rate of the electronic moments is lower.

We also carried out longitudinal-field (LF) μ^+ SR measurements on $\text{CuVOF}_4(\text{H}_2\text{O})_6 \cdot \text{H}_2\text{O}$ at $T = 1.2$ K for $0.5 \leq B \leq 2000$ mT ($B = \mu_0 H$) to investigate the spin dynamics. The field dependence of the LF relaxation rate can be used to determine the nature of transport of the spin excitations (i.e., ballistic or diffusive) as the spin autocorrelation functions have different spectral densities in the two cases. For one-dimensional (1D) diffusive transport, the spectral density $f(\omega)$ has the form $f(\omega) \sim \omega^{-1/2}$ [46], which leads to a $\lambda \propto B^{-1/2}$ power-law relation. In contrast, for ballistic transport, $f(\omega)$ follows a logarithmic relation $f(\omega) \propto \ln(c/\omega)$, or $\lambda \propto \ln(c/B)$, where c is a constant. In our case, for applied fields greater than 20 mT, above which the relaxation due to quasistatic nuclear moments is sufficiently quenched, the field dependence of the relaxation rate is well described by a power-law fit of the form $\lambda = aB^{-n}$ (see Fig. 7). We note that neither a logarithmic field-dependence describing ballistic spin transport (or 2D diffusive transport [46]) nor

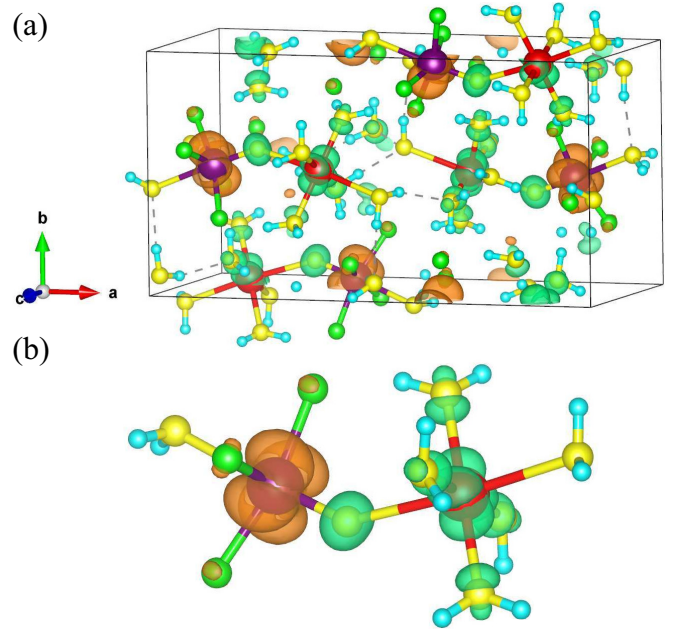


FIG. 8. Spin density distribution for the ground-state magnetic structure obtained from DFT. Orange and green isosurfaces represent regions with significant up and down spin density, respectively. (b) View of a single dimer in an antiferromagnetic configuration. The color coding of the atoms here is the same as it is in Fig. 1.

a Redfield model [45], appropriate for a dense array of randomly, dynamically fluctuating spins, can accurately describe the data. We obtain an exponent $n = 0.38(4)$, which is in reasonable agreement with the theoretical value $n = 0.5$ for 1D diffusive transport and similar to the values $n = 0.35$ and $n = 0.42$ measured for the 1D Heisenberg antiferromagnetic chain compounds DEOCC-TCNQF_4 [47] and $\text{Cu}(\text{pyz})(\text{NO}_3)_2$ [48], respectively, suggesting that the low frequency excitations in our material at this temperature are diffusive and primarily constrained to one dimension. Diffusive spin excitations are possible at low energy in an exchange-coupled network in general terms, owing to conservation laws for the components of magnetization and energy. Although one would not expect diffusion in a system of isolated dimers, the existence of the interdimer coupling in this system might allow such long-wavelength excitations to occur and explain the behavior we have observed.

E. Density functional theory

To identify the significant exchange pathways within the system, we carried out spin-polarized density functional theory (DFT+ U) calculations using the plane-wave basis-set electronic structure code CASTEP [49]. Details of these calculations can be found in the SM [20] alongside Refs. [49–63]. The spin-density distribution for the ground-state magnetic structure identified by our calculations is shown in Fig. 8. As shown in Fig. 8(a), the spins of the Cu and V ions within a dimer are aligned antiferromagnetically, Cu and V spins belonging to neighboring dimers are also aligned antiferromagnetically. As a result, the magnetic ground state can be thought of as comprising interpenetrating Cu and V

ferromagnetic sublattices. In Fig. 8(b) we show the spin density distribution across a single dimer when the system is in the ground state. There is significant spin density on the Cu and V ions and also on the O atom joining the Cu and V within a dimer, with this spin density having the opposite sign to the V ion within the dimer. As anticipated from the crystal structure, DFT finds that the magnetic orbitals of the Cu ion lie along the Cu–O bonds within the Jahn-Teller plane, inducing spin density in these O atoms. On the other hand, the O atoms on either end of the dimer carry very little spin density. For the V ion, the magnetic orbitals lie in-between the V–F bonds and the spin density on the F atoms is relatively small. The central O atom lies along the JT axis of the Cu ion, suggesting that its spin instead results from an AFM interaction with the V atom, with which it shares a short bond (≈ 1.6 Å).

By considering the DFT energies corresponding to several collinear spin configurations, we calculated the exchange constants associated with each of the exchange pathways. The calculated exchange constants depend very strongly on the value used for the Hubbard U , as has previously been found for systems based on Cu [56] and V [64]. For $U = 5$ eV on both the Cu and V d orbitals, we obtained a value $J_0 = 24.7(6)$ K for the intradimer exchange, which is broadly consistent with the experimental value. This value of U results in an interdimer coupling constant $J' = 8.6(15)$ K for the exchange within the bc plane, which is significantly larger than experiment, though we note that smaller values of J' are obtained when using larger values of U (see the SM [20]). The interdimer exchange along a between Cu and V ions on adjacent dimers [likely via the H bonds shown in Fig. 2(e)] was found to be < 0.6 K and hence its sign cannot be determined unambiguously within the uncertainties associated with these calculations. (Any coupling along a between two Cu, or two V, ions on adjacent dimers would be expected to be even weaker, as these H-bond pathways involve one or multiple JT or pseudo-JT axes.) These results show that each dimer couples antiferromagnetically to its four nearest neighbors in the bc plane, with only very weak coupling between dimers along the a -axis direction. This is in agreement with the exchange network posited from inspecting the structure.

More insight into how the magnetism in this system derives from the electronic structure can be obtained from the spin-polarized band structure and density of states (DOS), shown for the ground state magnetic configuration in Fig. 9. We note that this band structure and DOS is not typical of those obtained for an AFM system (see, for example, those for other AFM configurations in Fig. S8 in the SM), which typically exhibit pairs of degenerate spin-up and spin-down bands, and equal DOS in the two spin channels. This is due to the fact that the spin centers in the present system belong to two distinct species, and in the ground state all of the spins belonging to the same species point in the same direction. Despite this, and the fact that the ordered moments on Cu and V are not equal, the integrated DOS of the occupied states in each spin channel is equal, such that the system has no net magnetization, consistent with ESR data and the absence of any hysteresis in $M(H)$ (Fig. S1 in [20]). Within 1 eV of the Fermi energy, the band structure is characterized by two sets of dispersionless bands, indicative of localized states, 0.4 eV above and below the Fermi energy, corresponding to states

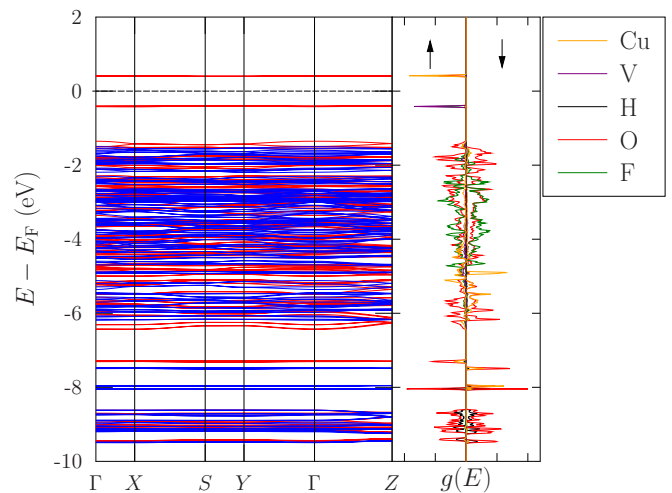


FIG. 9. Spin-polarized band structures for each of the magnetic ground state and the density of states for each spin channel. Bands corresponding to spin-up and spin-down are indicated by red and blue lines, respectively. The density of states are shown projected onto each atomic species.

localized on V and Cu, respectively. The V-centered states also have contributions from the F atoms the V is bonded to, while the Cu-centered states have contributions from the O atoms lying in the JT plane. These localized Cu and V states occupy the same spin channel despite the system being in an antiferromagnetic state. We can rationalize this by noting that these Cu orbitals are unoccupied and it is instead occupied Cu states that lie well below the Fermi energy that give rise to the moments on the Cu. These form part of an overlapping set of bands located around 2 to 6 eV below the energy and are not as well localized as the unoccupied Cu states. As we discuss later, these lower-lying Cu states are likely to play a key role in determining the magnetism in this system.

To more directly assess the exchange between pairs of magnetic ions, we devised a tight-binding model using Wannier orbitals derived from the two sets of four bands just below and above the Fermi energy (the construction of this model is described in detail in the SM [20]). Our model therefore includes eight Wannier orbitals, with four centered on Cu ions and four centered on V ions, as shown in Fig. 10. A tight-binding model constructed from these Wannier orbitals,

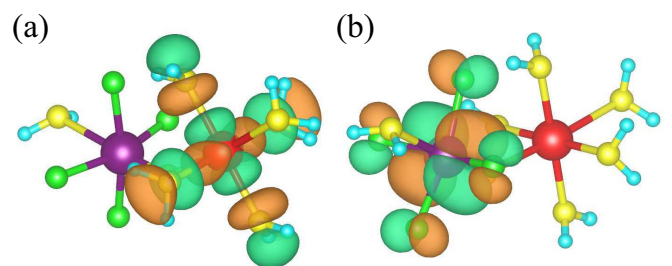


FIG. 10. The two distinct classes of maximally localized Wannier functions, which are localized either on (a) Cu or (b) V. Orange and green isosurfaces correspond to positive and negative values for the Wannier function, respectively.

including only those overlaps corresponding to hopping between nearest-neighbor ions, is able to successfully reproduce the main features of these bands. Within this model, the intradimer hopping $t = 2.87$ meV (33.3 K) is found to be nearly an order of magnitude smaller than the effective interdimer hopping $t' = 17.1$ meV (198.4 K) between dimers in bc plane (variations in the interdimer hopping are discussed in detail in the SM). The relative sizes of these hopping deviate strongly from the calculated and experimental exchange constants, but can be explained from the shapes of the Wannier orbitals. Both Cu- and V-centered orbitals lie perpendicular to the dimers and therefore the overlap between orbitals on adjacent dimers within the bc plane is much stronger than the overlap between orbitals along the dimer. We note that a similar tight-binding model based on Wannier orbitals was able to describe the magnetic interactions in copper-pyrazine antiferromagnets [65]. However, in those systems superexchange is mediated by pyz ligands lying in the JT plane, with the shapes of the Wannier orbitals reflecting this. This is in stark contrast to our system, where the principal exchange is along the JT axis, and where it appears that the magnetism cannot be accurately described by considering only hopping between localized orbitals near the Fermi energy.

Taken together, the results of this suite of calculations indicate that the magnetism in this system cannot be simply described in terms of superexchange between localized Cu and V orbitals. While the occupied V orbitals are highly localized and close to the Fermi energy, the Cu orbitals that give Cu its magnetic moment lie among a set of overlapping bands much further below the Fermi energy. The DFT total-energy approach used to calculate exchange constants takes into account all of the electrons in the system and yields exchange constants that are qualitatively consistent with those from experiment, unlike the hopping parameters derived from our tight-binding model, which instead suggests intradimer exchange should be dominant. It is therefore likely other atoms within the dimer play a key role in determining the magnitude of the intradimer exchange. This is likely to include the central O atom joining Cu and V atoms within a dimer, as this atom is found to have a significant spin density and could therefore be responsible for mediating the exchange within a dimer.

III. DISCUSSION

The positions of $H_{c1,2}$ obtained from the magnetometry experiments show some dependence on the orientation of the sample relative to the applied magnetic field, which we ascribe predominantly to g -factor anisotropy. Our orientation-dependent ESR measurements enable us to determine g factors for measurements made with an applied field along all three principal crystallographic axes [20]. Scaling our values of $H_{c1,2}$ measured with $H \perp a$ using $g_b = 2.046$ and plotting them as $(g_b/g_a)\mu_B B_{c1,2}$ (where $B_{c1,2} = \mu_0 H_{c1,2}$), we find that the values of $H_{c1,2}$ for both orientations very nearly coincide with one another as shown in Fig. 11. The red 2 K datapoint (measured with $H \parallel a$) indicates the upper temperature limit for the existence of the triplet excited state, as estimated using RF susceptometry. Reference [66] permits one to estimate the upper temperature limit of the XY -AFM ordered state to be

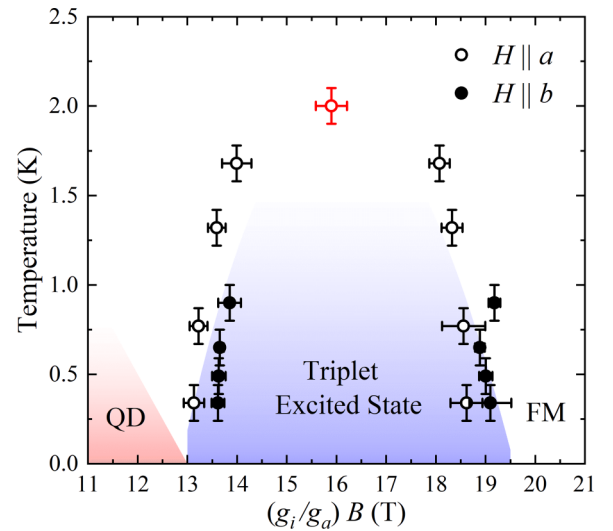


FIG. 11. Temperature-field phase diagram for $\text{CuVOF}_4(\text{H}_2\text{O})_6 \cdot \text{H}_2\text{O}$ where g_i denotes g factors with field along $i = a, b$ as described in the text. Blue shaded region serves as a guide to the eye to highlight phase boundaries that enclose the excited triplet state. Red shaded region indicates the quantum disordered (QD) state at fields below H_{c1} while FM indicates the ferromagnetically saturated state above H_{c2} . Upper limit for the dome marked with red circle at $T = 2.0(1)$ K.

$T_{\max} \approx nJ'/4$, which for our material returns $T_{\max} \approx 1.4(2)$ K, which is in reasonable agreement with our susceptometry evidence that the dome closes within the temperature region $1.6 < T < 2.0$ K.

Despite correcting for g -factor anisotropy, a slight anisotropy is still observed between similar temperature $H_{c1,2}$ values determined with $H \parallel a$ and $H \parallel b$. The cause of this may be the smearing out of the positions of $H_{c1,2}$ due to dislocations in the extensive H-bond network, as described above. The lack of an inversion center between the Cu and V ions may also permit the existence of a small DMI, which could lead to an additional orientation dependence of $H_{c1,2}$ [7,11].

The temperature-field phase diagram in Fig. 11 is a result of both the intradimer exchange J_0 and the interdimer exchange J' . As $\chi(T)$, ESR and DFT calculations suggest J' is AFM, at low-temperature the critical fields relate to J_0 and J' via [66]

$$g\mu_B B_{c1} = J_0 - nJ'/2, \quad g\mu_B B_{c2} = J_0 + nJ', \quad (3)$$

where $n = 4$ is the number of nearest dimer neighbors, as determined from DFT calculations.

Using the critical field values at $T = 0.34$ K and g factors from ESR, Eqs. (3) return parameters of $J_0 = 22.1(6)$ K and $J' = 1.4(2)$ K ($n = 4$), in excellent agreement with $\chi(T)$ and ESR. The system can therefore be well approximated using an isotropic dimer model with weak interdimer interactions [66].

As described above, crystal architectures composed of JT-active Cu(II) octahedra have previously been shown to promote low-dimensional magnetic behavior [24,67–69]. The $d_{x^2-y^2}$ orbital of the Cu lies within a plane perpendicular to the JT axis, resulting in minimal orbital overlap between

adjacent Cu ions bonded along a JT axis, and hence very weak magnetic exchange in this direction. This is reflected in our DFT calculations [Fig. 8(b)], which show an increased spin density, arising from the $d_{x^2-y^2}$ orbital, along the equatorial Cu–OH₂ bonds, perpendicular to the axial O–Cu–OH₂ JT bond direction.

Similarly, the presence of a pseudo-JT distortion in six-coordinate V(IV) ($3d^1$) complexes can also facilitate the emergence of low-dimensional magnetism [70,71]. For non-polar octahedra, an axial elongation results in the $3d^1$ electron occupying the degenerate d_{xz} and d_{yz} orbitals, while an axial compression leads to the $3d^1$ electron inhabiting the d_{xy} orbital. (Typically, axial compression is favored in $3d^1$ octahedra, as occupying the d_{xy} orbital offers the greater energy saving compared to occupying one of the degenerate d_{xz} or d_{yz} orbitals [72].) In the present case, the shortened V=O double-bond [1.6083(8) Å] and elongated V–OH₂ bond [2.2903(7) Å] of the polar VF₄O₂ octahedra makes it difficult to ascertain which orbital the $3d^1$ electron occupies by inspecting the structure alone. However, DFT calculations in Fig. 8(b) show an increased spin density between the V–F ligands in the *bc* plane, indicative that the $3d^1$ electron occupies the d_{xy} orbital.

As anticipated, DFT calculations find negligible spin-density located on the axial water ligand of either the Cu or V octahedra. Therefore, while the axial waters do form H bonds between adjacent dimers along *a*, the interdimer magnetic exchange will occur primarily within the *bc* plane via the H-bond network outlined in Fig. 1(d). Furthermore, the only H-bond pathway along *a* which is not via an axial water [blue-striped bonds, Fig. 1(e)] is found by DFT to mediate a vanishingly weak exchange, such that the system can be considered to be a magnetically 2D network of $S = 1/2$ dimers.

The interdimer exchange within this 2D network (*bc* plane) is estimated to be $J' \approx 1$ K, while the intradimer exchange is determined to be much greater at $J_0 \approx 21$ K. Therefore, the exchange pathway which mediates J_0 must be considerably more efficient than the J' exchange pathways. The interdimer Cu–O–H...F–V bonds which mediate J' fall within the range 6.51–6.656 Å, which is very similar in length to the intradimer Cu–O–H...F–V bond 6.553 Å [Fig. 2(c)]. It is therefore unlikely the strong J_0 is mediated along the intradimer H-bond pathway. Instead it seems apparent that the bridging oxide, which DFT shows as harboring significant spin-density and which is located along the JT axis of the Cu, is involved in mediating the intradimer exchange. For the reasons outlined above, significant exchange through a JT bond is very rare. However, a similar scenario has been encountered once before in the 2D AFM chain compounds CuX₂(pyz); where X = Cl, Br, F [73–75]. In this case, however, magnetic exchange is mediated along Cu–X₂–Cu bibridges, for which only one of the X–Cu–X bridges lies along the JT axial direction, while the other lies in the plane containing the $d_{x^2-y^2}$ magnetic orbital [75]. This means that, in the present case, the manner in which the intradimer exchange is mediated through the O atom on the Cu(II) JT axis remains unusual [76].

The two distinct $S = 1/2$ species in CuVOF₄(H₂O)₆ · H₂O exhibit very different behavior, with the occupied magnetic orbitals for V being highly localized states located just below the Fermi energy, whereas the occupied Cu states lie significantly lower in energy and are more delocalized. The tight-binding model, based on Wannier orbitals localized around the Cu and V, successfully reproduces the electronic band structure of the system in the vicinity of the Fermi energy, but fails to accurately describe the magnetic properties of the system. In contrast, DFT calculations, which also consider the delocalized bands below the Fermi energy, are able to qualitatively describe the magnetism within the compound. We hypothesise that the strong V=O double bond allows the vanadyl species to donate a sizable portion of its spin density to the bridging oxide, leading to the Cu and V ions coupling antiferromagnetically, via the delocalized bands below the Fermi energy, to form an AFM spin-half dimer. This demonstrates that the JT distortion, coupled with the unlike nature of the spin species, is not only responsible for the polar crystal structure [9] but also, by driving the formation of the Cu–O=V bond, establishes the effective intradimer exchange pathway within the dimer units. This is completely different to the usual way in which JT physics drives low-dimensional magnetism in other Cu(II) systems.

ACKNOWLEDGMENTS

This project has received funding from the European Research Council (ERC) under the European Union's Horizon 2020 research and innovation program (Grant Agreement No. 681260). S.P.M.C. and P.A.G. thank Alix McCollam, Thomas Khouri, and John Singleton for valuable discussions. We thank T. Orton and P. Ruddy for technical assistance. This work is supported by the EPSRC (under Grants No. EP/N032128/1 and No. EP/N024028/1). We thank the STFC-ISIS facility for the provision of muon beamtime and K. J. A. Franke and M. C. Worsdale for experimental assistance. We acknowledge computing resources provided by STFC Scientific Computing Department's SCARF cluster and Durham Hamilton HPC. Work at EWU was supported by the National Science Foundation under Grant No. DMR-1703003. A portion of this work was performed at the National High Magnetic Field Laboratory, which is supported by the National Science Foundation Cooperative Agreement No. DMR-1644779 and the State of Florida. D.K. was supported by the PRIME program of the German Academic Exchange Service (DAAD) with funds from the German Federal Ministry of Education and Research (BMBF). This work was carried out by the joint research program of Molecular Photoscience Research Center, Kobe University, and supported by KAKENHI from Japan Society for the Promotion of Science: Grants No. 19K21852 (H.O.) and No. 19K03746 (T.S.). We would like to acknowledge the members of the X-ray Diffraction Research Technology Platform at The University of Warwick for their assistance with the work described in this paper. Data presented in this paper resulting from the UK effort will be made available at [82].

- [1] P. Gegenwart, Q. Si, and F. Steglich, *Nat. Phys.* **4**, 186 (2008).
- [2] O. Stockert and F. Steglich, *Annu. Rev. Condens. Matter Phys.* **2**, 79 (2011).
- [3] V. Zapf, M. Jaime, and C. D. Batista, *Rev. Mod. Phys.* **86**, 563 (2014).
- [4] T. Lancaster, P. A. Goddard, S. J. Blundell, F. R. Foronda, S. Ghannadzadeh, J. S. Möller, P. J. Baker, F. L. Pratt, C. Baines, L. Huang, J. Wosnitza, R. D. McDonald, K. A. Modic, J. Singleton, C. V. Topping, T. A. W. Beale, F. Xiao, J. A. Schlueter, A. M. Barton, R. D. Cabrera *et al.*, *Phys. Rev. Lett.* **112**, 207201 (2014).
- [5] T. Giamarchi, C. Rüegg, and O. Tchernyshyov, *Nat. Phys.* **4**, 198 (2008).
- [6] A. Zheludev and T. Roscilde, *C. R. Phys.* **14**, 740 (2013).
- [7] K. Nawa, C. Michioka, K. Yoshimura, A. Matsuo, and K. Kindo, *J. Phys. Soc. Jpn.* **80**, 034710 (2011).
- [8] S. E. Sebastian, P. Tanedo, P. A. Goddard, S.-C. Lee, A. Wilson, S. Kim, S. Cox, R. D. McDonald, S. Hill, N. Harrison, C. D. Batista, and I. R. Fisher, *Phys. Rev. B* **74**, 180401(R) (2006).
- [9] M. D. Donakowski, R. Gautier, J. Yeon, D. T. Moore, J. C. Nino, P. S. Halasyamani, and K. R. Poeppelmeier, *J. Am. Chem. Soc.* **134**, 7679 (2012).
- [10] T. Moriya, *Phys. Rev.* **120**, 91 (1960).
- [11] M. Kofu, H. Ueda, H. Nojiri, Y. Oshima, T. Zenmoto, K. C. Rule, S. Gerischer, B. Lake, C. D. Batista, Y. Ueda, and S.-H. Lee, *Phys. Rev. Lett.* **102**, 177204 (2009).
- [12] A. A. Aczel, Y. Kohama, M. Jaime, K. Ninos, H. B. Chan, L. Balicas, H. A. Dabkowska, and G. M. Luke, *Phys. Rev. B* **79**, 100409(R) (2009).
- [13] M. Jaime, V. F. Correa, N. Harrison, C. D. Batista, N. Kawashima, Y. Kazuma, G. A. Jorge, R. Stern, I. Heinmaa, S. A. Zvyagin, Y. Sasago, and K. Uchinokura, *Phys. Rev. Lett.* **93**, 087203 (2004).
- [14] H. Nojiri, H. Kageyama, K. Onizuka, Y. Ueda, and M. Motokawa, *J. Phys. Soc. Jpn.* **68**, 2906 (1999).
- [15] T. Rõõm, D. Hüvonen, U. Nagel, J. Hwang, T. Timusk, and H. Kageyama, *Phys. Rev. B* **70**, 144417 (2004).
- [16] Z. Wang, M. Schmidt, Y. Goncharov, Y. Skourski, J. Wosnitza, H. Berger, H.-A. Krug von Nidda, A. Loidl, and J. Deisenhofer, *J. Phys. Soc. Jpn.* **80**, 124707 (2011).
- [17] D. Kamenskyi, J. Wosnitza, J. Krzystek, A. A. Aczel, H. A. Dabkowska, A. B. Dabkowski, G. M. Luke, and S. A. Zvyagin, *J. Low Temp. Phys.* **170**, 231 (2013).
- [18] Z. Wang, D. Kamenskyi, O. Cépas, M. Schmidt, D. L. Quintero-Castro, A. T. M. N. Islam, B. Lake, A. A. Aczel, H. A. Dabkowska, A. B. Dabkowski, G. M. Luke, Y. Wan, A. Loidl, M. Ozerov, J. Wosnitza, S. A. Zvyagin, and J. Deisenhofer, *Phys. Rev. B* **89**, 174406 (2014).
- [19] Z. Wang, M. Schmidt, A. Günther, F. Mayr, Y. Wan, S.-H. Lee, H. Ueda, Y. Ueda, A. Loidl, and J. Deisenhofer, *Phys. Rev. B* **85**, 224304 (2012).
- [20] See Supplemental Material at <http://link.aps.org/supplemental/10.1103/PhysRevB.104.214435> for experimental details and further analysis of magnetometry, μ^+ SR, ESR, and DFT.
- [21] Rigaku, <https://www.rigaku.com/products/crystallography/synergys>.
- [22] CrysAlispro, CrysAlisPRO, Oxford Diffraction /Agilent Technologies UK Ltd, Yarnton, England.
- [23] G. M. Sheldrick, *Acta Crystallogr. Sect. C* **71**, 3 (2015).
- [24] J. L. Manson, J. A. Schlueter, K. A. Funk, H. I. Southerland, B. Twamley, T. Lancaster, S. J. Blundell, P. J. Baker, F. L. Pratt, J. Singleton, R. D. McDonald, P. A. Goddard, P. Sengupta, C. D. Batista, L. Ding, C. Lee, M.-H. Whangbo, I. Franke, S. Cox, C. Baines *et al.*, *J. Am. Chem. Soc.* **131**, 6733 (2009).
- [25] B. M. Huddart, J. Brambleby, T. Lancaster, P. A. Goddard, F. Xiao, S. J. Blundell, F. L. Pratt, J. Singleton, P. Macchi, R. Scatena, A. M. Barton, and J. L. Manson, *Phys. Chem. Chem. Phys.* **21**, 1014 (2019).
- [26] A. Lanza, C. Fiolka, M. Fisch, N. Casati, M. Skoulatos, C. Rüegg, K. W. Krämer, and P. Macchi, *Chem. Commun.* **50**, 14504 (2014).
- [27] O. V. Kravchina, A. I. Kaplienko, E. P. Nikolova, A. G. Anders, D. V. Ziolkovskii, A. Orendachova, and M. Kajnakova, *Russian J. Phys. Chem. B* **5**, 209 (2011).
- [28] A. A. Aczel, Y. Kohama, C. Marcenat, F. Weickert, M. Jaime, O. E. Ayala-Valenzuela, R. D. McDonald, S. D. Selesnic, H. A. Dabkowska, and G. M. Luke, *Phys. Rev. Lett.* **103**, 207203 (2009).
- [29] R. Feyerherm and S. Abens, *J. Phys.: Condens. Matter* **12**, 8495 (2000).
- [30] J. Liu, S. Kittaka, R. D. Johnson, T. Lancaster, J. Singleton, T. Sakakibara, Y. Kohama, J. van Tol, A. Ardavan, B. H. Williams, S. J. Blundell, Z. E. Manson, J. L. Manson, and P. A. Goddard, *Phys. Rev. Lett.* **122**, 057207 (2019).
- [31] G. J. Athas, J. S. Brooks, S. J. Klepper, S. Uji, and M. Tokumoto, *Rev. Sci. Instrum.* **64**, 3248 (1993).
- [32] T. Coffey, Z. Bayindir, J. F. DeCarolis, M. Bennett, G. Esper, and C. C. Agosta, *Rev. Sci. Instrum.* **71**, 4600 (2000).
- [33] R. B. Clover and W. P. Wolf, *Rev. Sci. Instrum.* **41**, 617 (1970).
- [34] J. Brambleby, P. A. Goddard, J. Singleton, M. Jaime, T. Lancaster, L. Huang, J. Wosnitza, C. V. Topping, K. E. Carreiro, H. E. Tran, Z. E. Manson, and J. L. Manson, *Phys. Rev. B* **95**, 024404 (2017).
- [35] S. Ghannadzadeh, M. Coak, I. Franke, P. A. Goddard, J. Singleton, and J. L. Manson, *Rev. Sci. Instrum.* **82**, 113902 (2011).
- [36] J. L. Manson, J. Brambleby, P. A. Goddard, P. M. Spurgeon, J. A. Villa, J. Liu, S. Ghannadzadeh, F. Foronda, J. Singleton, T. Lancaster, S. J. Clark, I. O. Thomas, F. Xiao, R. C. Williams, F. L. Pratt, S. J. Blundell, C. V. Topping, C. Baines, C. Campana, and B. Noll, *Sci. Rep.* **8**, 4745 (2018).
- [37] T. Nakajima, H. Mitamura, and Y. Ueda, *J. Phys. Soc. Jpn.* **75**, 054706 (2006).
- [38] S. A. Zvyagin, M. Ozerov, D. Kamenskyi, J. Wosnitza, J. Krzystek, D. Yoshizawa, M. Hagiwara, R. Hu, H. Ryu, C. Petrovic, and M. E. Zhitomirsky, *New J. Phys.* **17**, 113059 (2015).
- [39] A. Ceulemans, L. F. Chibotaru, G. A. Heylen, K. Pierloot, and L. G. Vanquickenborne, *Chem. Rev.* **100**, 787 (2000).
- [40] M. Kofu, J.-H. Kim, S. Ji, S.-H. Lee, H. Ueda, Y. Qiu, H.-J. Kang, M. A. Green, and Y. Ueda, *Phys. Rev. Lett.* **102**, 037206 (2009).
- [41] M. Matsumoto, T. Shoji, and M. Koga, *J. Phys. Soc. Jpn.* **77**, 074712 (2008).
- [42] S. J. Blundell, *Contemp. Phys.* **40**, 175 (1999).
- [43] S. Blundell, R. De Renzi, T. Lancaster, and F. Pratt, *Muon Spectroscopy: An Introduction* (Oxford University Press, Oxford, 2021).

- [44] P. D. de R  otier and A. Yaouanc, *J. Phys.: Condens. Matter* **9**, 9113 (1997).
- [45] R. S. Hayano, Y. J. Uemura, J. Imazato, N. Nishida, T. Yamazaki, and R. Kubo, *Phys. Rev. B* **20**, 850 (1979).
- [46] M. A. Butler, L. R. Walker, and Z. G. Soos, *J. Chem. Phys.* **64**, 3592 (1976).
- [47] F. L. Pratt, S. J. Blundell, T. Lancaster, C. Baines, and S. Takagi, *Phys. Rev. Lett.* **96**, 247203 (2006).
- [48] F. Xiao, J. S. M  ller, T. Lancaster, R. C. Williams, F. L. Pratt, S. J. Blundell, D. Ceresoli, A. M. Barton, and J. L. Manson, *Phys. Rev. B* **91**, 144417 (2015).
- [49] S. J. Clark, M. D. Segall, C. J. Pickard, P. J. Hasnip, M. I. Probert, K. Refson, and M. C. Payne, *Z. Krist.* **220**, 567 (2005).
- [50] E. Ruiz, J. Cano, S. Alvarez, and P. Alemany, *J. Comput. Chem.* **20**, 1391 (1999).
- [51] E. Ruiz, A. Rodr  guez-Forteza, J. Cano, S. Alvarez, and P. Alemany, *J. Comput. Chem.* **24**, 982 (2003).
- [52] R. L. Martin and F. Illas, *Phys. Rev. Lett.* **79**, 1539 (1997).
- [53] L. H. Dos Santos, A. Lanza, A. M. Barton, J. Brambleby, W. J. Blackmore, P. A. Goddard, F. Xiao, R. C. Williams, T. Lancaster, F. L. Pratt, S. J. Blundell, J. Singleton, J. L. Manson, and P. Macchi, *J. Am. Chem. Soc.* **138**, 2280 (2016).
- [54] J. P. Perdew, K. Burke, and M. Ernzerhof, *Phys. Rev. Lett.* **77**, 3865 (1996).
- [55] H. J. Monkhorst and J. D. Pack, *Phys. Rev. B* **13**, 5188 (1976).
- [56] I. O. Thomas, S. J. Clark, and T. Lancaster, *Phys. Rev. B* **96**, 094403 (2017).
- [57] N. Marzari and D. Vanderbilt, *Phys. Rev. B* **56**, 12847 (1997).
- [58] I. Souza, N. Marzari, and D. Vanderbilt, *Phys. Rev. B* **65**, 035109 (2001).
- [59] G. Pizzi, V. Vitale, R. Arita, S. Bl  gel, F. Freimuth, G. G  ranton, M. Gibertini, D. Gresch, C. Johnson, T. Koretsune, J. Iba  nez-Azpiroz, H. Lee, J.-M. Lihm, D. Marchand, A. Marrazzo, Y. Mokrousov, J. I. Mustafa, Y. Nohara, Y. Nomura, L. Paulatto *et al.*, *J. Phys.: Condens. Matter* **32**, 165902 (2020).
- [60] G. Prandini, A. Marrazzo, I. E. Castelli, N. Mounet, and N. Marzari, *npj Comput. Mater.* **4**, 72 (2018).
- [61] E. Kucukbenli, M. Monni, B. I. Adetunji, X. Ge, G. A. Adebayo, N. Marzari, S. de Gironcoli, and A. D. Corso, [arXiv:1404.3015](https://arxiv.org/abs/1404.3015).
- [62] K. F. Garrity, J. W. Bennett, K. M. Rabe, and D. Vanderbilt, *Comput. Mater. Sci.* **81**, 446 (2014).
- [63] A. Dal Corso, *Comput. Mater. Sci.* **95**, 337 (2014).
- [64] A. A. Tsirlin and H. Rosner, *Phys. Rev. B* **79**, 214417 (2009).
- [65] E. P. Kenny, A. C. Jacko, and B. J. Powell, *Inorg. Chem.* **60**, 11907 (2021).
- [66] M. Tachiki and T. Yamada, *J. Phys. Soc. Jpn.* **28**, 1413 (1970).
- [67] S. Ghannadzadeh, J. S. M  ller, P. A. Goddard, T. Lancaster, F. Xiao, S. J. Blundell, A. Maisuradze, R. Khasanov, J. L. Manson, S. W. Tozer, D. Graf, and J. A. Schlueter, *Phys. Rev. B* **87**, 241102(R) (2013).
- [68] Z. Wang, P. Jain, K.-Y. Choi, J. van Tol, A. K. Cheetham, H. W. Kroto, H.-J. Koo, H. Zhou, J. Hwang, E. S. Choi, M.-H. Whangbo, and N. S. Dalal, *Phys. Rev. B* **87**, 224406 (2013).
- [69] J. Brambleby, P. A. Goddard, R. D. Johnson, J. Liu, D. Kaminski, A. Ardavan, A. J. Steele, S. J. Blundell, T. Lancaster, P. Manuel, P. J. Baker, J. Singleton, S. G. Schwalbe, P. M. Spurgeon, H. E. Tran, P. K. Peterson, J. F. Corbey, and J. L. Manson, *Phys. Rev. B* **92**, 134406 (2015).
- [70] T. Waki, M. Kato, Y. Itoh, C. Michioka, K. Yoshimura, and T. Goto, *J. Phys. Chem. Solids* **66**, 1432 (2005).
- [71] O. Mentr  , A. C. Dhaussy, F. Abraham, E. Suard, and H. Steinfink, *Chem. Mater.* **11**, 2408 (1999).
- [72] M. Dalal, *A Textbook of Inorganic Chemistry – Volume 1* (Amazon Digital Services LLC - KDP Print US, 2017), pp. 312–321.
- [73] R. T. Butcher, C. P. Landee, M. M. Turnbull, and F. Xiao, *Inorganica Chim. Acta* **361**, 3654 (2008).
- [74] S. H. Lapidus, J. L. Manson, J. Liu, M. J. Smith, P. Goddard, J. Bendix, C. V. Topping, J. Singleton, C. Dunmars, J. F. Mitchell, and J. A. Schlueter, *Chem. Commun.* **49**, 3558 (2013).
- [75] T. Lancaster, B. M. Huddart, R. C. Williams, F. Xiao, K. J. A. Franke, P. J. Baker, F. L. Pratt, S. J. Blundell, J. A. Schlueter, M. B. Mills, A. C. Maahs, and K. E. Preuss, *J. Phys.: Condens. Matter* **31**, 394002 (2019).
- [76] A number of papers do report Cu(II)—O=V(IV) linkages in various other materials (see, e.g., [77–81]). However, we can find no discussion of the role of the Jahn-Teller axis in mediating exchange through this pathway and there remains no clear quantitative evidence for significant antiferromagnetic coupling between Cu(II) and V(IV) in these compounds.
- [77] R. C. Finn, R. Lam, J. E. Greedan, and J. Zubieta, *Inorg. Chem.* **40**, 3745 (2001).
- [78] X.-M. Zhang, H.-S. Wu, S. Gao, and X.-M. Chen, *J. Solid State Chem.* **176**, 69 (2003).
- [79] M. E. Welk, C. L. Stern, K. R. Poeppelmeier, and A. J. Norquist, *Cryst. Growth Des.* **7**, 956 (2007).
- [80] X. Wu, T. Huang, T. T. Lekich, R. D. Sommer, and W. W. Weare, *Inorg. Chem.* **54**, 5322 (2015).
- [81] J. C. Trombe, P. Rozier, and J. Galy, *Acta Crystallogr. Sect. C* **59**, i50 (2003).
- [82] <http://wrap.warwick.ac.uk/160275/>.